NAVAL POSTGRADUATE SCHOOL
MONTEREY, CALIFORNIA

THESIS

FURTHER INVESTIGATION OF THE SCATTERING OF UNDERWATER SOUND FROM A POROUS SOLID SPHERE

by

Martin E. Pace

December 1994

Thesis Advisor: S.R. Baker

Approved for public release; distribution is unlimited

REPORT DOCUMENTATION PAGE

Form Approved
OMB No. 0704-0188

1. AGENCY USE ONLY *(Leave blank)*

2. REPORT DATE
December 1994

3. REPORT TYPE AND DATES COVERED
Master's Thesis

4. TITLE AND SUBTITLE
Further Investigation of the Scattering of Underwater Sound from a Porous Solid Sphere

5. FUNDING NUMBERS

6. AUTHOR(S)
Pace, Martin E.

7. PERFORMING ORGANIZATION NAME(S) AND ADDRESS(ES)
Naval Postgraduate School
Monterey CA 93943-5000

8. PERFORMING ORGANIZATION REPORT NUMBER

9. SPONSORING/MONITORING AGENCY NAME(S) AND ADDRESS(ES)

10. SPONSORING/MONITORING AGENCY REPORT NUMBER

11. SUPPLEMENTARY NOTES
The views expressed in this thesis are those of the author and do not reflect the official policy or position of the Department of Defense or the U.S. Government.

12a. DISTRIBUTION/AVAILABILITY STATEMENT
Approved for public release; distribution is unlimited.

12b. DISTRIBUTION CODE

13. ABSTRACT *(maximum 200 words)*

This investigation is an attempt to verify the results of a theoretical model, developed by Kargl and Lim, for the scattering of sound from a poro-elastic sphere embedded in a poro-elastic host. It is a follow-on to that conducted by LT. Theodore W. L. Huskey. Both monostatic and bistatic measurements were taken on two porous glass spheres composed of 100 and 500 μm glass beads and on an aluminum sphere. The Poisson's Ratio was calculated from the shear and Young's moduli measured from a cylindrical sample composed of 300 μm glass beads. This was used to calculate the bulk moduli for the porous spheres; the shear moduli had been previously measured by LT. Huskey. These and other material properties were used as input to the theoretical model developed by Kargl and Lim.

The experimental data were compared to the theoretical values. Reasonably good agreement between the measured and predicted scattering was obtained for the aluminum and 100 μm spheres. The measured scattering from the 500 μm sphere was in poor agreement with the theoretical predictions.

14. SUBJECT TERMS
Biot, Porous Medium, Backscatter, Borosilicate

15. NUMBER OF PAGES
53

16. PRICE CODE

17. SECURITY CLASSIFICATION OF REPORT	18. SECURITY CLASSIFICATION OF THIS PAGE	19. SECURITY CLASSIFICATION OF ABSTRACT	20. LIMITATION OF ABSTRACT
Unclassified	Unclassified	Unclassified	UL

NSN 7540-01-280-5500

Standard Form 298 (Rev. 2-89)
Prescribed by ANSI Std. 239-18

Approved for public release; distribution is unlimited.

FURTHER INVESTIGATION OF THE SCATTERING OF UNDERWATER SOUND FROM A POROUS SOLID SPHERE

Martin E. Pace
Lieutenant, United States Navy
B.S., Oregon State University, 1987

Submitted in partial fulfillment of the
requirements for the degree of

MASTER OF SCIENCE IN APPLIED PHYSICS

from the

NAVAL POSTGRADUATE SCHOOL
December 1994

Author: Martin E. Pace
Martin E. Pace

Approved by: Steven R Baker
S. R. Baker, Thesis Advisor

C. Scandrett, Second Reader

W. B. Colson
William B. Colson, Chairman, Department of Physics

ABSTRACT

This investigation is an attempt to verify the results of a theoretical model, developed by Kargl and Lim, for the scattering of sound from a poro-elastic sphere embedded in a poro-elastic host. It is a follow-on to that conducted by LT. Theodore W. L. Huskey. Both monostatic and bistatic measurements were taken on two porous glass spheres composed of 100 and 500 μm glass beads and on an aluminum sphere. The Poisson's Ratio was calculated from the shear and Young's moduli measured from a cylindrical sample composed of 300 μm glass beads. This was used to calculate the bulk moduli for the porous spheres; the shear moduli had been previously measured by LT. Huskey. These and other material properties were used as input to the theoretical model developed by Kargl and Lim.

The experimental data were compared to the theoretical values. Reasonably good agreement between the measured and predicted scattering was obtained for the aluminum and 100 μm spheres. The measured scattering from the 500 μm sphere was in poor agreement with the theoretical predictions.

TABLE OF CONTENTS

ACKNOWLEDGMENTS

The author wants to sincerely thank Prof. Steve Baker for his guidance and patience during the work in performing this investigation. I would also like to thank Steve Kargl of the University of Washington, Applied Physics Laboratory, for his assistance in my research.

I. INTRODUCTION

A. BACKGROUND

Because of the increased emphasis on littoral warfare and the threat of the use of buried mines in these areas, there is increased interest in the scattering of sound in fluid-saturated porous media.

Maurice Biot (Biot, 1956a, b) developed a general theory for the propagation of elastic waves in a fluid-saturated porous media. Biot's theory has been applied to the scattering of elastic waves from a saturated porous sphere in a saturated porous host (Kargl and Lim, 1993).

In 1993, LT. Huskey performed experiments in an attempt to verify Kargl and Lim's model. The results of his experiment were good when 10% frame damping was included in the calculations. Other calculations were less satisfactory. (Huskey, 1993)

B. OBJECTIVES

Kargl and Lim developed a numerical model to compute the scattering of sound from a saturated porous sphere. This research is an attempt to experimentally measure the scattering of sound from a saturated porous sphere and compare the results with the numerical values obtained from Kargl and Lim's model (Kargl and Lim, 1993).

C. EXPERIMENT OVERVIEW

As stated above, the purpose of this research is to measure the scattering of sound from a fluid saturated porous sphere. The spheres which were used in this research were composed of borosilicate glass beads. The beads had a mean diameter of 100 μm and 500 μm. The beads were coated with a heat curing epoxy powder and then poured into cylindrical molds. These molds were then heated to cure the epoxy. The resulting cylinders were ground into spheres with a diameter of about 6.8 centimeters. Cylindrical

rods composed of 100 μm and 500 μm glass beads were made at the same time as the spheres. These rods were used by LT. Huskey to measure the permeability, porosity, and shear modulus of the porous matrices. These values are summarized in Table 1 (Huskey, 1993).

Sample	100 μm	500 μm
Permeability, k	6.53×10^{-12} m^2	5.74×10^{-11} m^2
Porosity, P	0.309	0.321
Shear Modulus, G	2.81×10^{9} Pa	2.72×10^{9} Pa

Table 1. Material measurements taken by LT. Huskey.

Scattering measurements taken for these spheres were compared to theoretical values determined by the model developed by Kargl and Lim. This model requires eleven material parameters to determine the scattered amplitude. The scattering solid provides five of these material parameters: mass density, bulk and shear moduli of the solid, and bulk and shear moduli of the porous lattice. Three material properties are determined by the structure of the porous lattice: tortuosity, permeability, and structural factor. The final three properties are of the bulk fluid: mass density, and the bulk and shear moduli. (Kargl and Lim). The program provided by Kargl used the bulk fluid's bulk modulus and viscosity to determine complex values for the bulk and shear moduli.

In this experiment all the material properties were accurately known with the exception of the bulk moduli of the spheres. This could not be measured by LT. Huskey at the time of his research (Huskey, 1993) due to the small aspect ratio (length to diameter) of the cylindrical samples. For this experiment a new cylinder of 300 μm diameter porous glass beads with greater aspect ratio was obtained so that the bulk and shear moduli could be determined. From these moduli the Poisson's Ratio can be determined which can then be used along with the shear moduli of the 100 and 500 μm samples to determine their bulk moduli. Once these parameters are determined they can

be used as input, along with the other known material properties, to Kargl and Lim's theoretical model and the results compared with the experimentally measured values.

II. DETERMINATION OF ELASTIC MODULI

A. RESONANT ACOUSTIC METHOD

The elastic moduli of a cylindrical sample can be obtained using a resonant acoustic method (Garrett, 1990). This method employs a transducer bonded to each end of a cylindrical sample which should have a length to diameter ratio >>1. The transducers are made from coiled magnet wire and are attached with epoxy. These are used to set up flexural, torsional, and longitudinal standing waves in the samples. The bars are positioned so that the transducers attached to the ends are centered between the pole faces of strong magnets. Depending on the orientation of the transducers to the pole pieces, any of the three vibrational modes can be selectively excited. Figure 1, from (Garret, 1990), illustrates the position of the magnet faces for the torsional and longitudinal modes. The fundamental frequency of each mode can be determined based on the length and boundary conditions of the sample. These frequencies can then be used to determine the moduli of the sample.

In the experiments conducted by LT. Huskey only the shear modulus could be measured due to the length to diameter ratio of the samples (about 3:1) which intensified electrical cross-talk between the attached transducers.

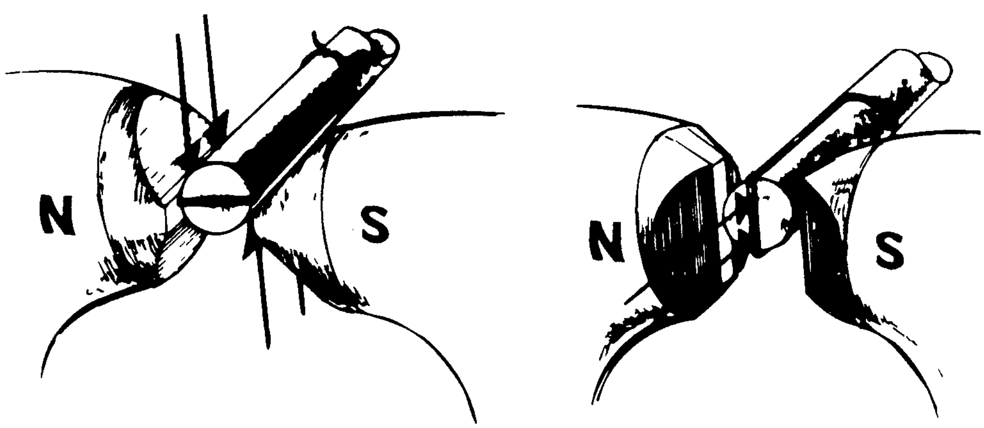

Figure 1. Transducer placement for the torsional and longitudinal modes.

B. ELASTIC MODULI MEASUREMENT

A sample made of 300 μm glass beads with a length of 19.7 centimeters and diameter of 2.6 centimeters (giving a length to diameter ratio of 7.6:1) was obtained and the resonant acoustic method was used to determine both the shear and bulk moduli of the sample. Approximately 2 meters of #32 magnet wire were attached to each end of the sample with epoxy resulting in 15 turns of wire in each transducer. Care was taken to minimize the amount of weight added by the epoxy. The sample weighed 153.52 grams and the transducers added 4.38 grams. The mass loading of the transducers was significant enough that an effective length of the bar had to be calculated using the following equations (Garret, 1990):

$$L_{eff} = L\left(1+\frac{m}{M}\right) \text{ (longitudinal mode)}$$

$$L_{eff} = L\left(1+\frac{2m}{M}\right) \text{ (torsional mode)}$$

where L is the actual length of the sample, m is the transducer mass, and M is the mass of the sample.

The sample was positioned so that each transducer was centered between the pole pieces of the magnets. One set of magnets were rotated 90° to minimize electrical cross-talk between the two transducers (one transducer was also offset 90° relative to the other when it was attached). A Hewlett-Packard 35665A Dynamic Signal Analyzer was used to drive one transducer through a Hewlett-Packard 467A Power Amplifier. The signal from the other transducer was then input to the Dynamic Signal Analyzer. Both signals were monitored on an oscilloscope to ensure that no distortion was occurring. The output from the Dynamic Signal Analyzer was then swept upward in frequency from 100 Hz to 20 kHz. The resonances were noted and the frequency bracket around each was tightened to allow for more accurate measurement of the resonance.

Mode Number, n	Modal Frequency Summary	
	Frequency (Hz), f_n	Normalized Frequency (Hz), f_n/n
Torsional		
1	2505	2505
2	5175	2588
3	7830	2610
4	10260	2565
Average		2567±45
Flexural		
1	3940	3940
2	8080	4040
3	11775	3925
4	15985	3996
Average		3975±53

Table 2. Resonant frequency measurements.

The first four modes of both the longitudinal and torsional modes were measured and averaged together. The results are shown in Table 2. The Young's modulus (E) of the sample was determined using the following equation (from Garrett):

$$E = 4\rho L_{eff}^{\ 2}\left(f_n^L/n\right)^2$$

where ρ is the mass density, n is the mode number, and f_n^L is the frequency of the nth longitudinal mode. The shear modulus (G) was similarly calculated using (from Garrett)

$$G = 4\rho L_{eff}^{\ 2}\left(f_n^T/n\right)^2$$

where f_n^T is the frequency of the nth torsional mode.

The calculated Young's modulus was 3.83×10^9 Pa and the shear modulus was 1.68×10^9 Pa. These values are approximately 1/20 of the borosilicate glass used to make the glass beads. These were used to calculate the Poisson's Ratio (ν) by combining

$$\nu = \frac{3K-2G}{2(3K+G)}$$

and
$$K = \frac{E}{3(1-2\nu)}$$

to give
$$\nu = \frac{E}{2G} - 1$$

	100 μm	500 μm
Shear Modulus, G, (from Huskey)	2.81×10^9 Pa	2.72×10^9 Pa
Bulk Modulus, K, assuming $\nu = 0.14$.	2.96×10^9 Pa	2.87×10^9 Pa

Table 3. Material properties of the samples.

where K is the bulk modulus. The resulting Poisson's Ratio was 0.14. This is an unusually small Poisson's Ratio and is possibly due to the epoxy used to bond the glass beads together. The epoxy may be stretching between the beads allowing the cylinder to elongate without much lateral constriction.

Since the 300 μm rod was made at a different time than the 100 μm and 500 μm spheres, the shear moduli measured by Huskey and the calculated Poisson's Ratio were used to calculate new bulk moduli for both spheres. These values are listed in Table 3 and were used as inputs to Kargl's program.

III. BACKSCATTER MEASUREMENTS

A. MEASUREMENT OBJECTIVE

The objective of the backscatter measurement was to separate the scattered acoustic pressure from the multipath interference. Multipath interference was caused by surface reflections from the transmitter's side lobes and from piping used for filtration of the tank's water.

B. EXPERIMENT SETUP

The backscatter measurements were taken in a water-filled tank, in Spanagel Hall Room 025, measuring 7.3 meters in length, 1.6 meters in width and 2.0 meters in depth. The walls and bottom of the tank are covered with anechoic tile. Figure 2 shows the tank setup for the backscatter measurements. All components were aligned along the centerline of the tank as viewed from the top of the tank.

A type F33 general-purpose directional transducer was used as the projector. This transducer is shown in Figure 3 from the *USRD Transducer Catalog*, April 1991. Its

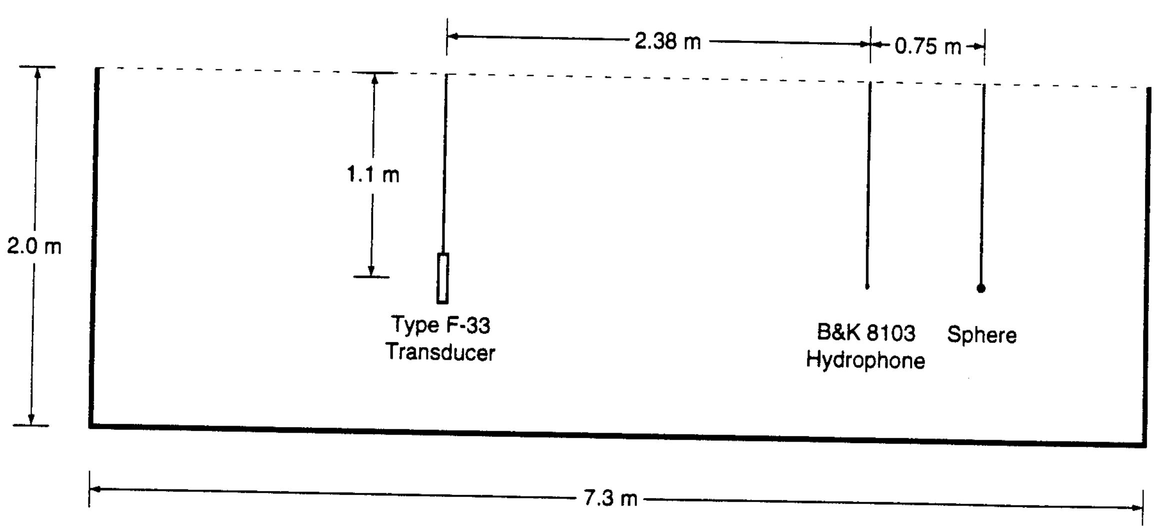

Figure 2. Tank setup for scattering measurements.

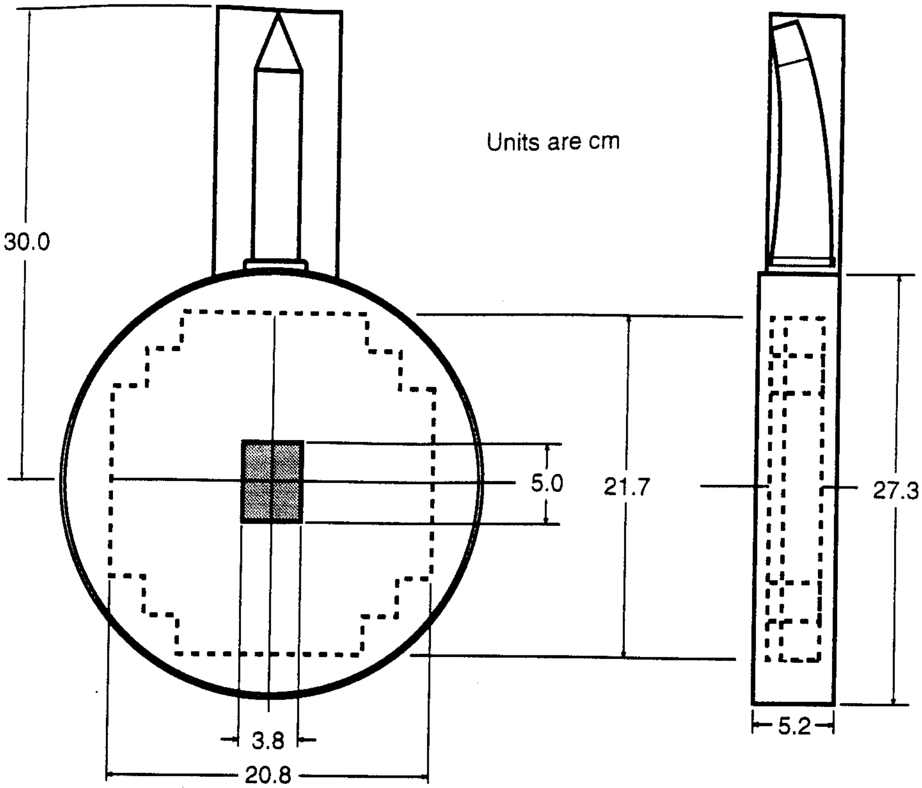

Figure 3. Type F33 general-purpose transducer.

design consists of a small inner array made of 12 PZT disks with a frequency range of 15-150 kHz. The larger outer array consists of 64 PZT squares with a frequency range of 1-50 kHz (*USRD Transducer Catalog*). The arrays can be used individually or wired in parallel. In this experiment the arrays were connected in parallel for added directionality.

To ensure accurate measurements, the scatterer must be placed in the far field of the transmitter. The following equation was used to determine the limiting distance to the far field (r_{min}):

$$r_{min} = \frac{1}{4}\frac{d^2}{\lambda}$$

where d is the dimension of the transmitter and λ is the wavelength of sound (Kinsler et al.). The lowest frequency used in this experiment was 30 kHz, giving a maximum distance to the far field of less than 0.25 meters.

The receiver used was a Bruel and Kjaer type 8103 hydrophone. Figure 4 shows an illustration of the receiver from its calibration chart. It has a frequency range of 0.1 to 180 kHz. The receiver was suspended from the arm of a protractor-like device illustrated in Figure 5. The arm can be rotated in five degree increments and locked into place with a lock pin. The 180° position corresponds to sound being scattered from the sphere directly back at the transmitter. The receiver could be moved radially, in increments of 5 centimeters, between 40 to 75 centimeters from the center of the protractor. A small clamp was attached to the cable of the hydrophone allowing the depth to be adjusted. The clamp rested in any one of several beveled holes in the protractor's arm. A weight was

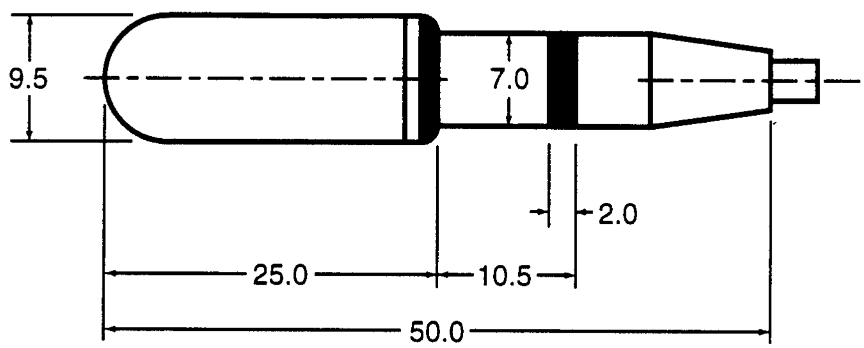

Units are mm

Figure 4. Bruel & Kjaer Type 8103 hydrophone.

suspended from the bottom of the receiver to ensure that it hung straight down. The weight was suspended a few centimeters from the bottom of the tank.

The target spheres were suspended in a fine net by a string. The string passed through a hole drilled in the bolt which was the pivot point of the protractor's arm. This allowed the depth of the sphere to be adjusted to correspond to the depth of the center of the transmitter. The spheres were degassed to ensure that no air bubbles were trapped in the spheres during the experimental measurements. This was done by placing them in a

beaker of water and then placing the beaker under a bell jar. A vacuum pump was then used to evacuate the bell jar until the water began to boil. At this point the hose to the bell jar was clamped and the vacuum pump was turned off. Periodically the beaker and sphere were agitated to dislodge any bubbles adhering to the surface. The vacuum was held for approximately 24 hours to ensure no bubbles remained trapped in the spheres. Next the hose clamp to the bell jar was removed allowing the pressure to return to normal. The bell jar was carefully removed and the sphere transported to the water tank in the beaker full of water. The beaker was submerged in the water tank and the sphere removed thus keeping it submerged at all times.

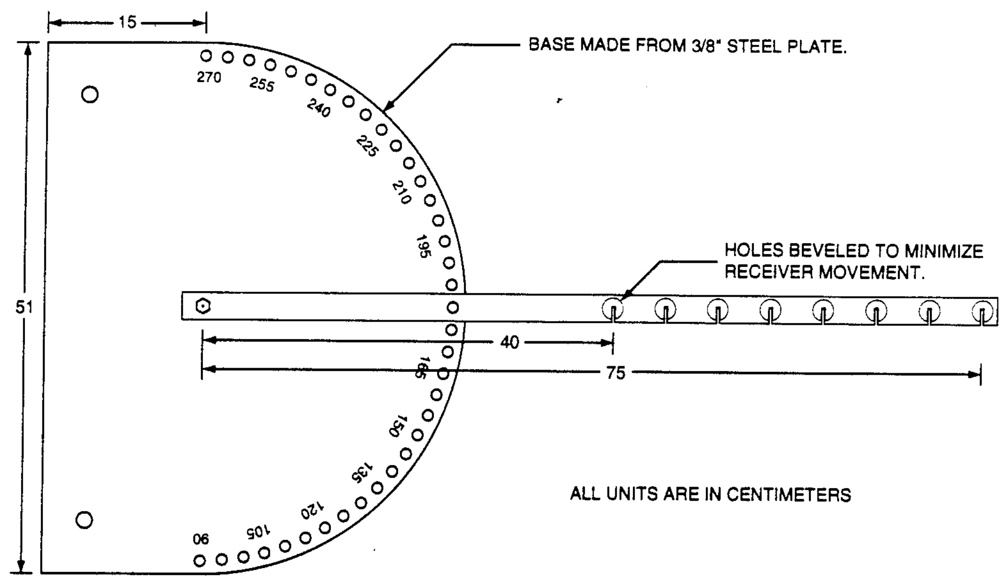

Figure 5. Protractor device used to position receiver.

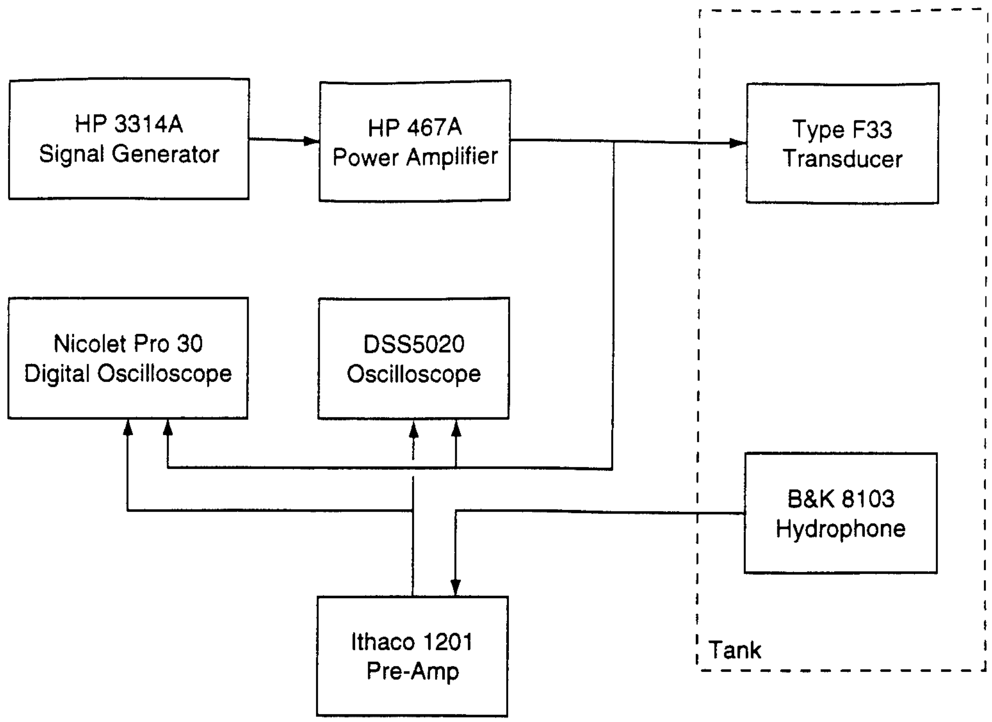

Figure 6. Electronic equipment setup.

Figure 6 is a block diagram of the electronics used for this experiment. A 1 Volt peak to peak sine wave was generated with the Hewlett-Packard 3314A Signal Generator which was then amplified to a 10 Volt peak to peak signal by a Hewlett-Packard 467A Power Amplifier. This signal was then applied to the Type F33 transducer. The signal could also be monitored by either the Nicolet Pro 30 Digital Oscilloscope or the DSS5020 Oscilloscope. The signal received by the Bruel & Kjaer 8103 hydrophone was input to an Ithaco 1201 Preamplifier. The output from the preamplifier was then analyzed by the Nicolet Pro 30 Oscilloscope.

C. EXPERIMENTAL PROCEDURE

The frequency range used for this experiment was 30 kHz to 150 kHz, corresponding to a range of ka of approximately 4 to 22, referred to the wave number in water.

1. Monostatic Measurements

For the monostatic measurements the sphere was hung below the protractor. The B&K hydrophone was positioned 75 centimeters from the sphere along the arm of the protractor which was positioned at 180°. The signal generator was setup to send out 30 kHz bursts at a rate of five bursts per second. Each burst consisted of a 30-cycle sine wave.

The Nicolet Pro 30 was used to monitor the received signal. A trigger delay was used so that the trace on the oscilloscope would begin just before the arrival of the scattered signal. The delay was determined by the speed of sound and the distance between the transmitter, sphere and receiver. The sample rate was set so that the pulse would fill as much of the oscilloscope's screen as possible without being cutoff. Careful attention was paid to ensure that the sample rate remained well above the Nyquist frequency of the received signal. Fifty bursts of the received signal were averaged together and then saved to floppy disk. Measurements were taken between 30 and 150 kHz in 2 kHz steps.

At this point the sphere was carefully removed from the tank to a bucket of water and the above procedure was repeated to obtain the multipath interference background in the tank. The next measurement to be taken was the incident signal on the sphere. Due to the design of the protractor, the B&K hydrophone could not be positioned in the same place as the sphere but had to be positioned 15 centimeters behind it. This displacement was taken into account in the calculations by using a 1/r signal fall-off in the far field of the transmitter (Kinsler et al.). The incident signal was measured at each frequency.

Once the received signal and multipath interference background measurements had been taken, the saved waveforms were subtracted from each other, leaving only the scattered pulse. The subtraction process was performed using the Nicolet Pro 30 Digital Oscilloscope. Figure 7 shows the measured signal, multipath interference background, and resulting scattered signal from the subtraction process.

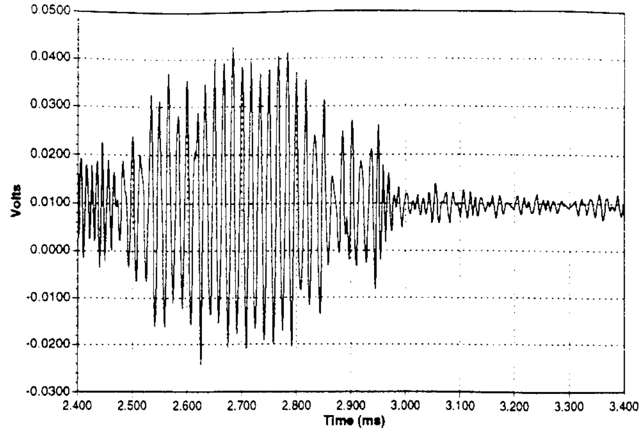

Measured signal.

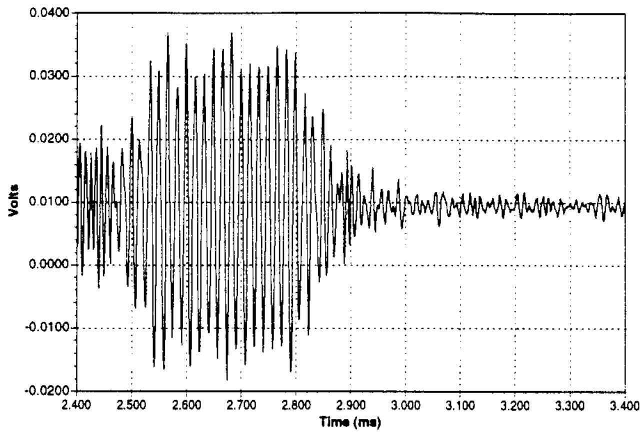

Multipath interference background signal.

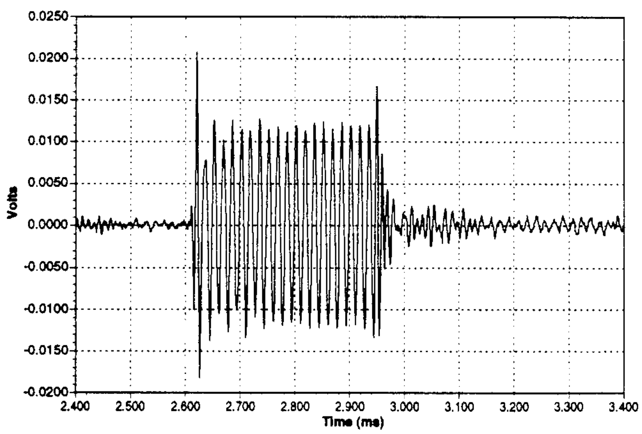

Scattered signal.

Figure 7. Example of subtracting the measured signal from the multipath interference background. At top is the received signal, in the middle is the multipath interference, and bottom is the difference between the measured signal and multipath interference background.

Next a Fast Fourier Transform (FFT) was taken of the scattered and incident waveforms, using the Nicolet Pro 30, to determine the amplitude of the desired transmitted frequency component. The start and stop points of the FFT were chosen so that they were inside the start and end points of the transmitted pulse. This was done to avoid distortion caused by the HP467A Power Amplifier turning on and off, and to avoid any ring up and down of the Type F33 transmitter. Care was taken to ensure that a whole number of wavelengths were taken and that the start and stop points were as close as possible to a zero crossing to avoid leakage into adjacent frequency bins when the FFT was taken (Hewlett-Packard, Application Note 243, pp. 25-26). No windowing function was used with the above method. The results of these measurements are listed in Appendix A. The method of calculation of the tabulated results are discussed in Chapter IV Section A, Normalization of Experimental Data.

2. Bistatic Measurements

Bistatic measurements were conducted in a manner similar to the monostatic measurements. The difference was that instead of adjusting the frequency between measurements, the angular position of the receiver was adjusted. The receiver was started in the 90° position and then moved in 5° increments until the 270° position was reached. The sphere was then removed from the tank and the background measurements were taken. Next the receiver was moved to measure the incident signal level on the sphere. After these measurements were made the resulting waveforms were subtracted and FFTs taken to obtain the scattered and incident signal levels. These measurements were performed at the following frequencies: 30, 60, 90, 120, and 150 kHz. Results of the measurements are listed in Appendix B.

For the aluminum sphere measurements were taken only at 30 kHz and 150 kHz since these were to be used as a gauge of the effectiveness of the experimental method.

IV. DATA ANALYSIS AND RESULTS

A. NORMALIZATION OF EXPERIMENTAL DATA

All of the experimental data was normalized to a distance of 1 meter from the sphere. This was done by using the following equation:

$$\text{Normalized Scattering} = \frac{V_{scattered} \times r}{V_{incident}}$$

where r is the distance between the sphere and the receiver and $V_{incident}$ is given by

$$V_{incident} = V'_{incident} \times \frac{R + 0.15}{R}$$

where $V'_{incident}$ is the measured incident signal (approximately 15 cm behind where the sphere actually was) and R is the transmitter to sphere distance.

B. THEORETICAL DATA

The values for the theoretical data were obtained from two FORTRAN programs provided by Kargl. One program calculates the theoretical monostatic data results and the other the bistatic results for a saturated poro-elastic sphere in a saturated poro-elastic medium.

The program requires almost 30 inputs. These inputs are the material properties of the external fluid and poro-elastic medium, both water in this experiment, and the internal fluid (water) and poro-elastic medium of the scatterer. The internal poro-elastic medium was either porous glass or the aluminum. Inputs to the programs can be found in Appendix C.

C. COMPARISON OF THEORETICAL AND EXPERIMENTAL DATA

1. Scattering from the Aluminum Sphere

Figure 8 shows a comparison of the theoretical and experimental data for monostatic scattering from the aluminum sphere. Experimental data points are marked by × and connected with a dashed line. The dashes are only to guide the eye and are not an attempt at a curve fit. After the experimental data were taken the sphere was weighed and measured to verify the properties for input into Kargl's program. It was found that the aluminum sphere weighed approximately 30% more than it should. The sphere was not a solid aluminum sphere, it was an aluminum shell covering a core of some heavier unknown material. The main features in the experimental data agree very well with the theoretical data below 90 kHz except that the experimental values are shifted to the right by 5–10 kHz. Beyond 90 kHz the features match in relative position but the experimental data has a lower amplitude. Figure 9 shows the data adjusted so that it spans 20 to 150 kHz. This shows a much better match between the theoretical and experimental values at frequencies below 90 kHz. Since the sphere was determined not to be solid aluminum these results are considered to be in reasonable agreement with the predicted values and show that the experimental procedure is valid.

For the bistatic case, shown in Figure 10 and Figure 11, the structure and amplitudes do not agree well. Again, this is not unexpected since the sphere was not solid aluminum. However, because the lobing is clearly defined in the experimental data, it was again considered that the experimental procedure was valid.

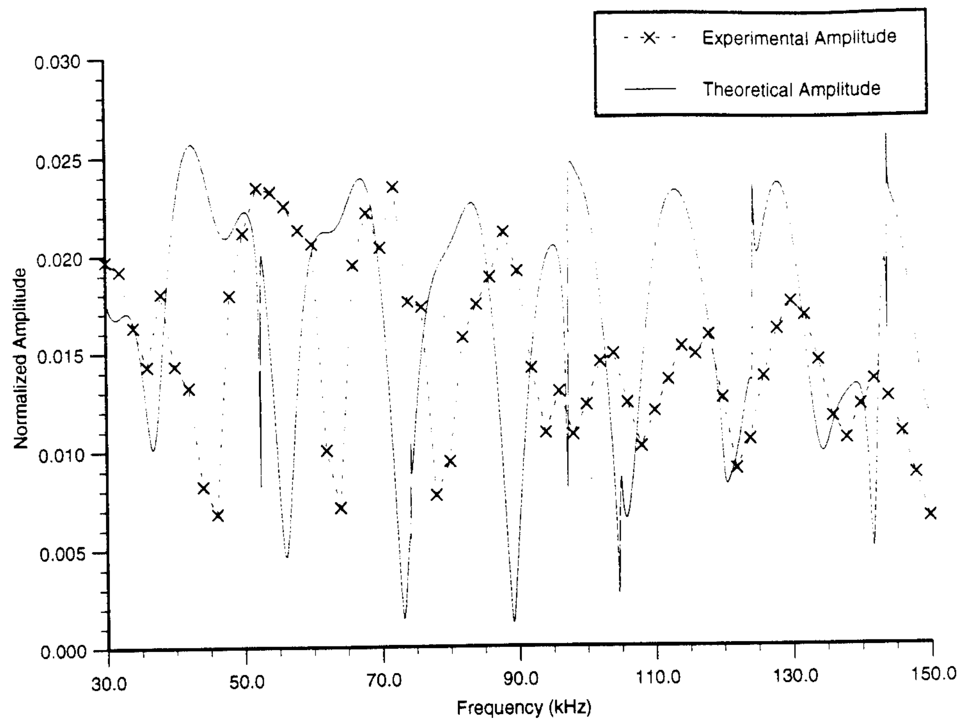

Figure 8. Normalized monostatic scattering amplitudes from the aluminum based sphere.

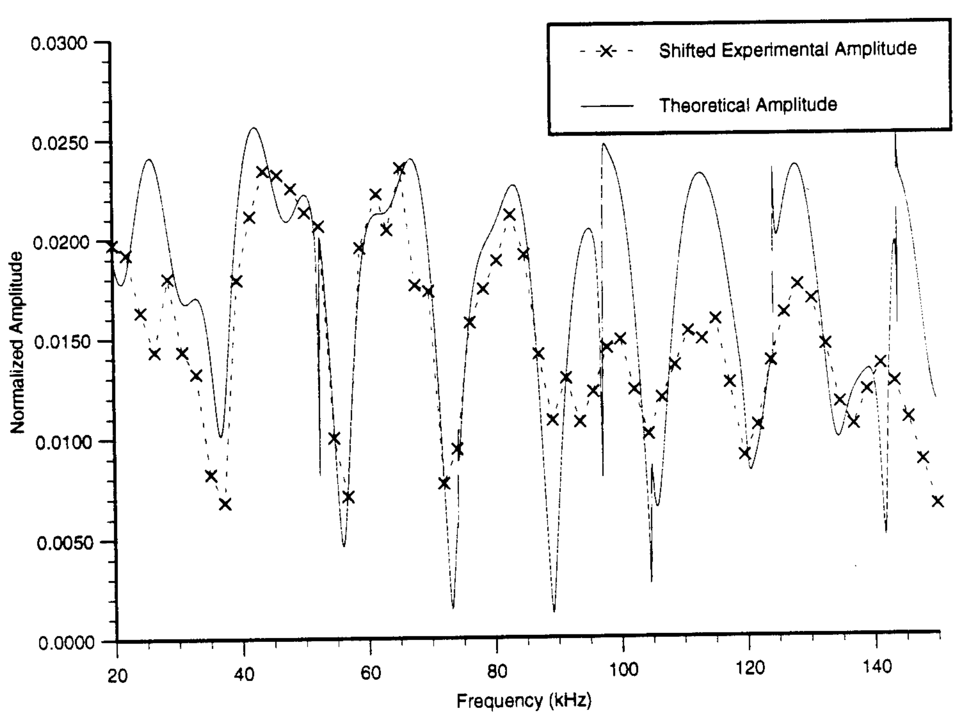

Figure 9. Normalized monostatic scattering amplitudes from the aluminum based sphere with data 'stretched' between 20 and 150 kHz.

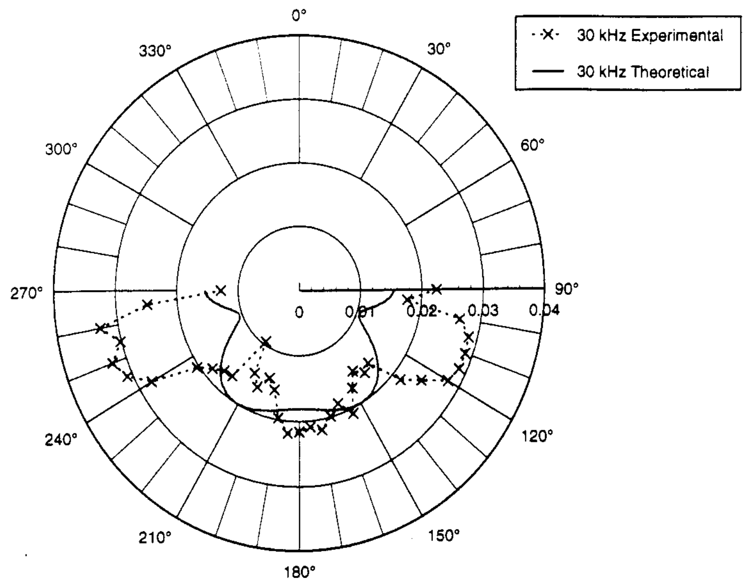

Figure 10. Normalized bistatic scattering at 30 kHz from aluminum sphere.

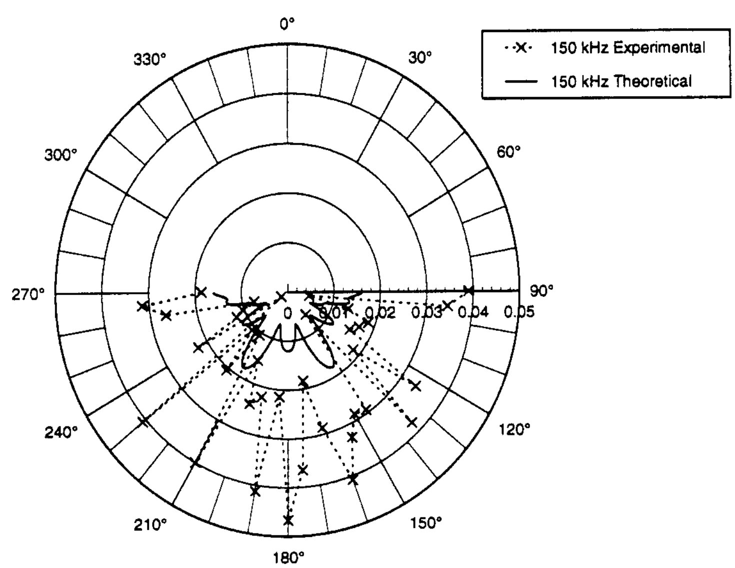

Figure 11. Normalized bistatic scattering at 150 kHz from aluminum sphere.

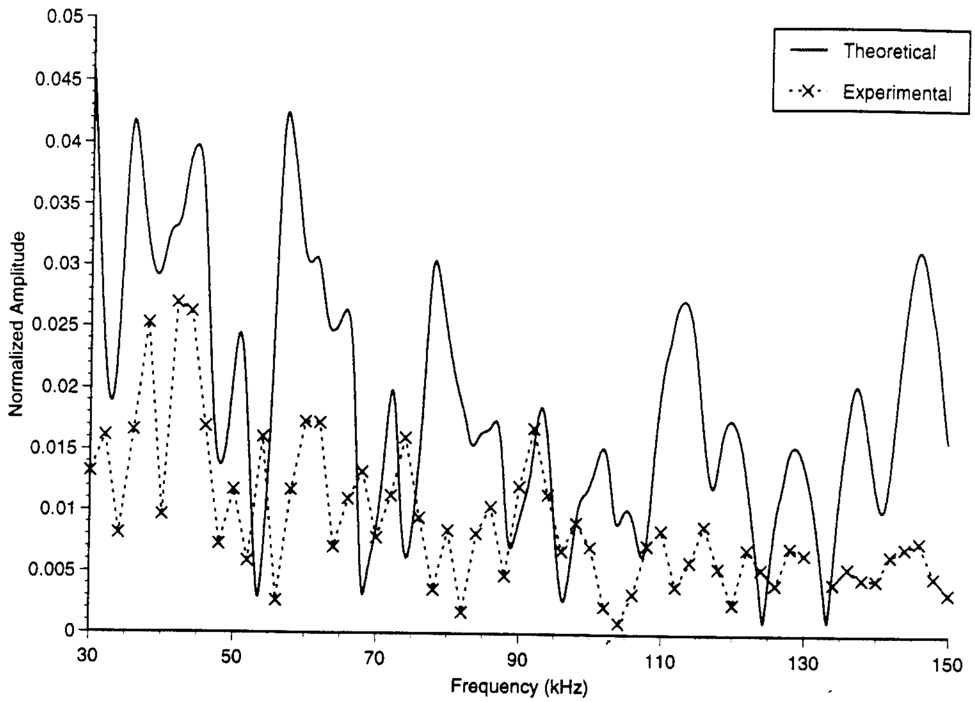

Figure 12. Normalized monostatic scattering amplitudes from the 100 μm sphere.

2. Scattering from the 100 μm Porous Glass Sphere

Figure 12 shows the results for monostatic scattering from the 100 μm sphere. Most of the features in the experimental data can be found to correspond fairly well to features in the theoretical model up to about 80 kHz and less so above 80 kHz. Note that the amplitude of the experimental data is lower than the theoretical data. This agrees with the bistatic data, which consistently shows that the amplitudes of the main lobes are lower than the theoretical prediction even when the side lobes have similar amplitudes as shown in Figures 13 through 17.

Figures 13 through 17 show the theoretical and experimental bistatic scattering data sets. There is good agreement for the 30, 60 and 90 kHz data sets except for the amplitudes of the main lobes. The 120 kHz data matches well and the 150 kHz data only

agrees in overall magnitude of the scattering. This is believed to be due to the increased sensitivity of the beam pattern to the material properties. In varying the values used as input for Kargl's program, it was noted that the beam pattern varied slightly at 30 kHz and increased in variation as frequency was increased. The resulting beam pattern varied significantly at 150 kHz. This is the most likely cause of the disagreement.

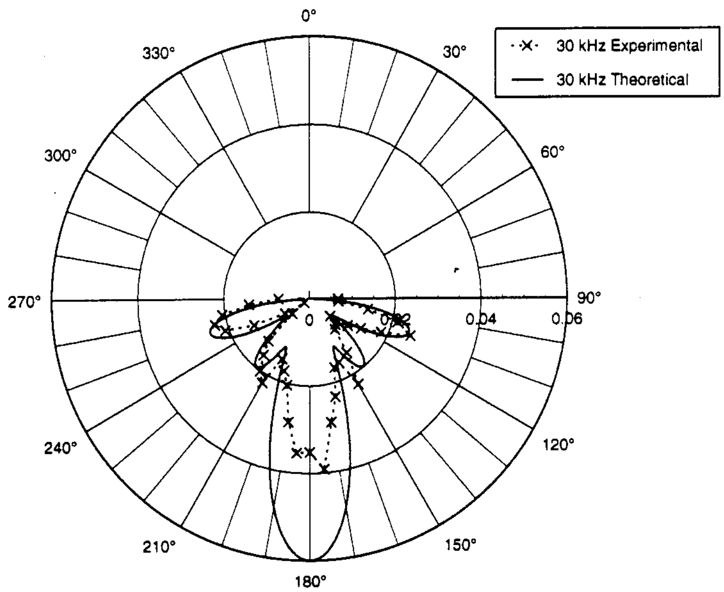

Figure 13. Normalized bistatic scattering at 30 kHz from 100 μm sphere.

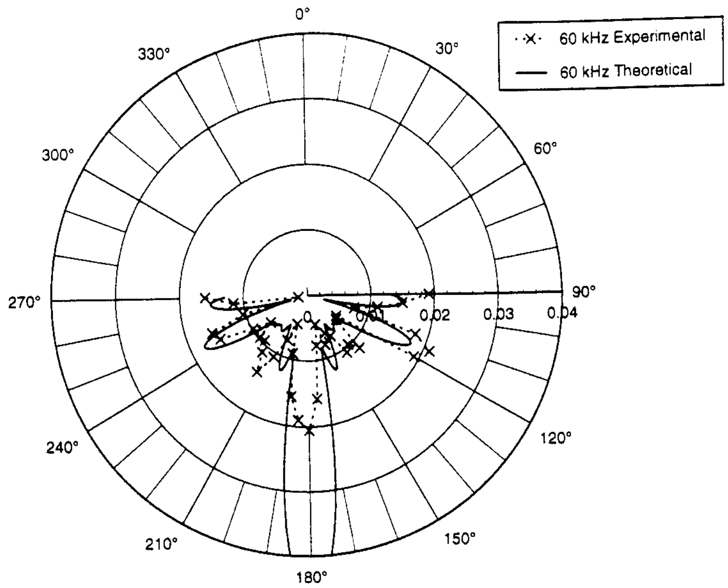

Figure 14. Normalized bistatic scattering at 60 kHz from 100 μm sphere.

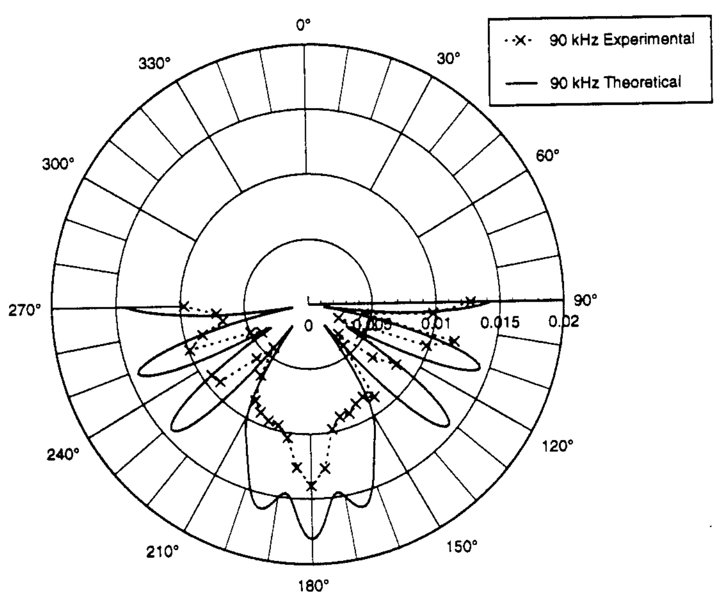

Figure 15. Normalized bistatic scattering at 90 kHz from 100 μm sphere.

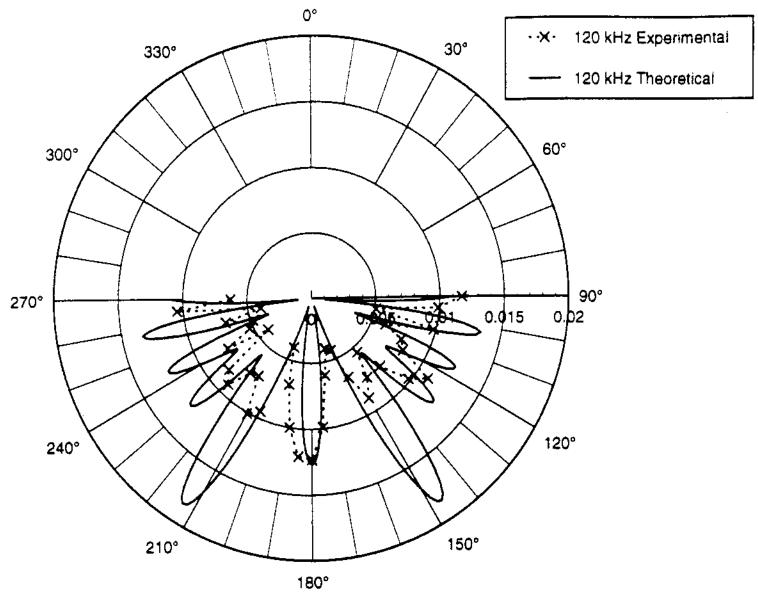

Figure 16. Normalized bistatic scattering at 120 kHz from 100 μm sphere.

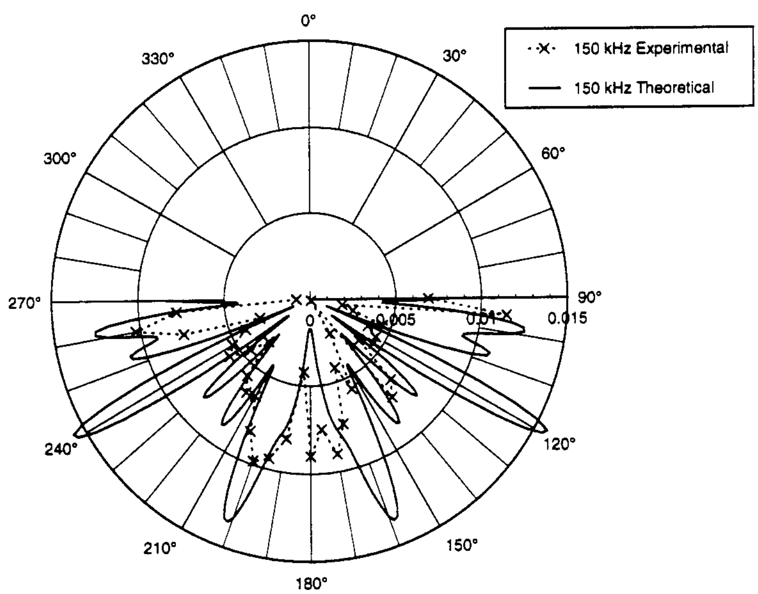

Figure 17. Normalized bistatic scattering at 150 kHz from 100 μm sphere.

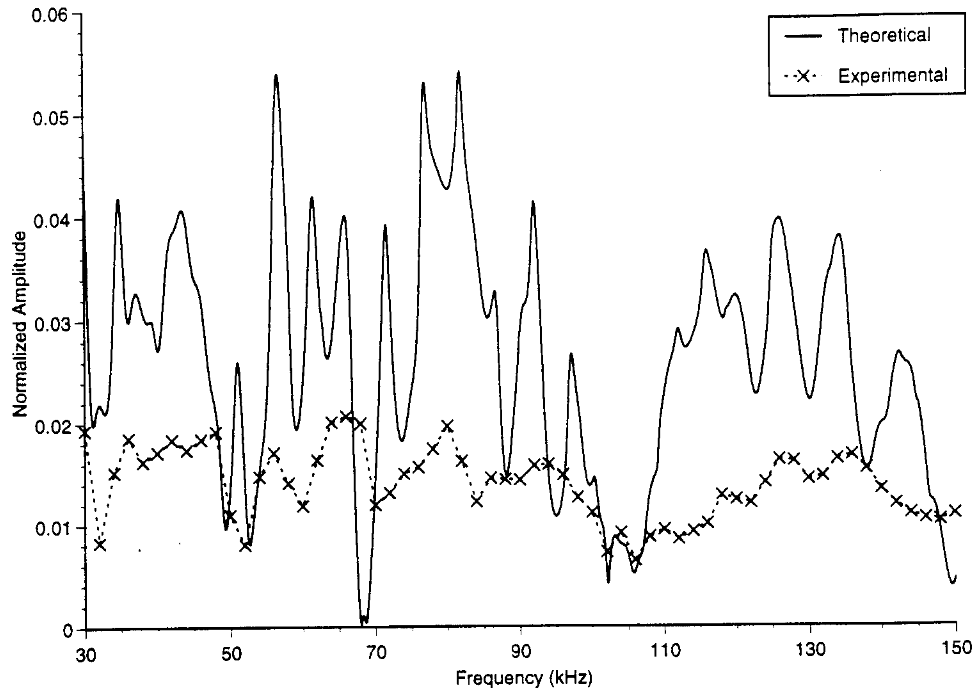

Figure 18. Normalized monostatic scattering from the 500 μm sphere.

3. Scattering from the 500 μm Porous Glass Sphere

Monostatic scattering for the 500 μm sphere is shown in Figure 18. It is possible to see some correspondence between features below 90 kHz but above this frequency no match can be found.

Figures 19 through 23 show the bistatic results for the 500 μm sphere. There is no correspondence between the experimental and theoretical values. It is believed that this is due to defects in the 500 μm sphere. Prior to the experiment it was noted that this sphere has a $0.9 \times 0.5 \times 0.25$ centimeter gouge in its surface. The surface is also less consistent in texture from one area to another. Also the surface is more susceptible to crumbling than the 100 μm sphere. Finally, both spheres were weighed and measured and their densities calculated. Both were found to have a density of about 1550 kg/m^3. This density

corresponds with the 100 μm bar used by LT. Huskey for determining the material properties of the 100 μm sphere. However, the density of the 500 μm bar used by LT. Huskey was 1513 kg/m^3 (Huskey, 1993) which is about 2.5% lower than for the 500 μm sphere.

Based on the material condition of the 500 μm sphere and on the good results obtained with the 100 μm sphere it is believed that the 500 μm sphere is defective and that this caused the disagreement between the theoretical and experimental data.

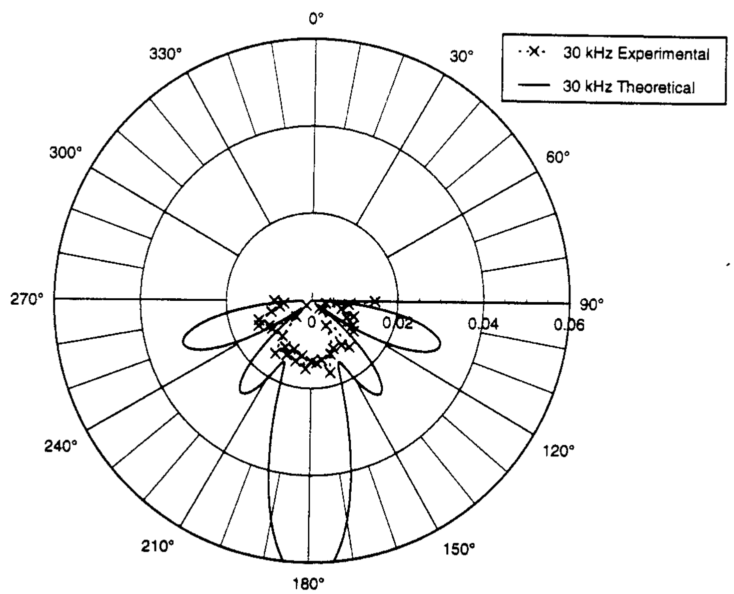

Figure 19. Normalized bistatic scattering at 30 kHz from 500 μm sphere.

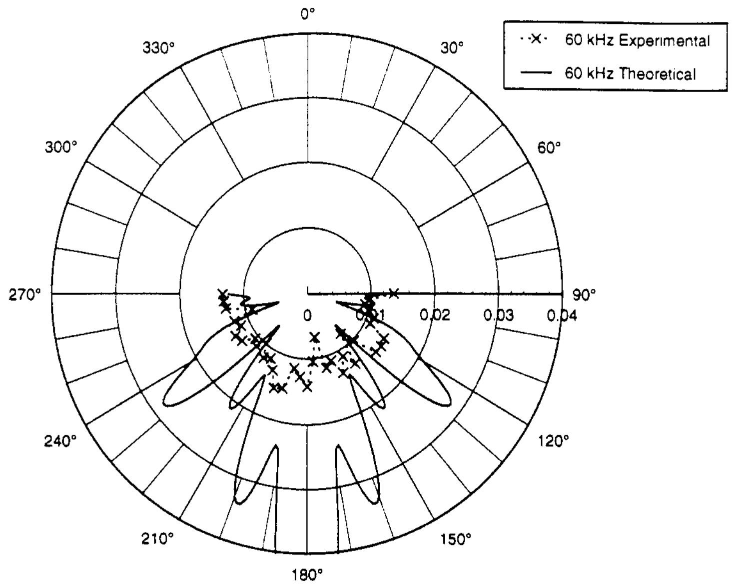

Figure 20. Normalized bistatic scattering at 60 kHz from 500 μm sphere.

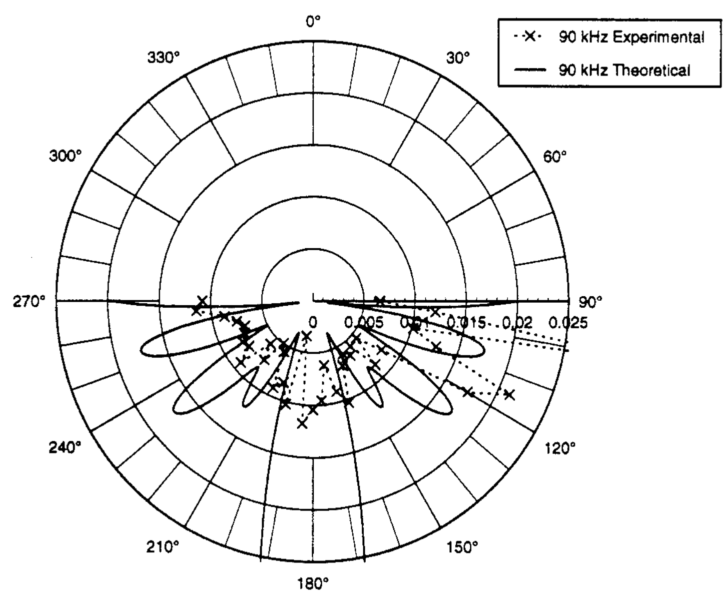

Figure 21. Normalized bistatic scattering at 90 kHz from 500 μm sphere.

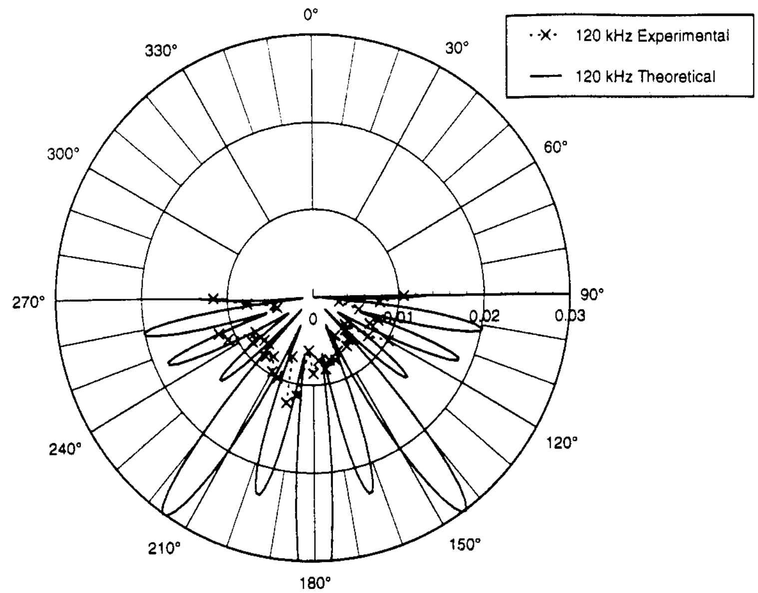

Figure 22. Normalized bistatic scattering at 120 kHz from 500 μm sphere.

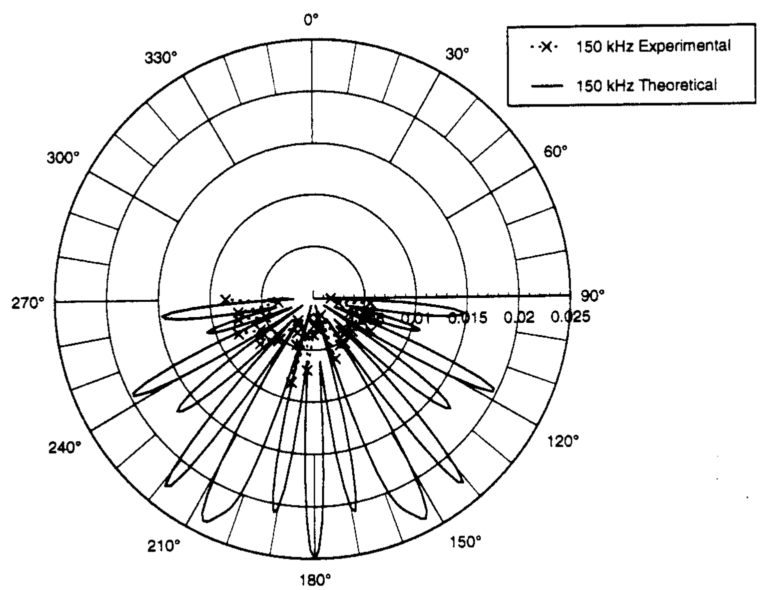

Figure 23. Normalized bistatic scattering at 150 kHz from 500 μm sphere.

V. CONCLUSION AND RECOMMENDATIONS

A. CONCLUSION

The scattering of sound from an aluminum based sphere and from porous glass spheres composed of 100 μm and 500 μm diameter glass beads was measured. Monostatic and bistatic measurements were made for backscatter at 30, 60, 90, 120 and 150 kHz. Experimental data were compared with theoretical data computed by a FORTRAN program written by Kargl. The program was based on the theory developed by Kargl and Lim for the scattering of sound from a fluid saturated poro-elastic sphere in a saturated poro-elastic medium.

Material properties of the spheres were measured for input into Kargl's program. The elastic moduli of a cylindrical bar composed of 300 μm diameter bonded glass beads were measured and used to determine the bar's Poisson's Ratio. This Poison's ratio was used to determine the value of the bulk moduli of the 100 μm and 500 μm porous glass spheres. Other material properties of these spheres had been previously measured by LT. Huskey.

Comparison of the experimental data to the theoretical from Kargl's program yielded reasonable results for the aluminum based sphere. Very good results were obtained for the 100 μm sphere. The measurements at the lower frequencies agreed more closely than those at the higher frequencies. This is due to the increased sensitivity of the spatial structure of the scattering at higher frequencies to slight variations in the material properties of the spheres. The main lobe was found to be lower in amplitude than predicted at all frequencies. No explanation of this could be found at this time. It is speculated that this may be the result of slight inhomogeneity in the composition of the sphere. At higher frequencies it may be due to error in the axial alignment of the source, sphere, and receiver. The 500 μm sphere produced extremely poor results and it is believed that this sphere is defective, specifically it is thought to be non-homogeneous.

B. RECOMMENDATIONS

Scattering measurements at lower frequencies is recommended. This would require a larger tank than is present at the Naval Postgraduate School. This would allow measurements to be made where the fluid's viscosity would affect the flow of the fluid through the pores in the spheres.

For measurements at higher frequencies the material properties of the spheres need to be known to fairly high accuracy. For this to be accomplished new spheres should be made at the same as the time cylindrical samples are made. The cylindrical samples should have a length to diameter ratio greater than 15:1 to allow accurate measurement of the elastic moduli. The surfaces of the cylinders should also be machined so that they are consistent with the sphere's surfaces. Also, for measurements at higher frequencies, a more accurate method for positioning the receiver is needed. Measurements should be taken at sufficiently small intervals to adequately define the structure of the side lobes.

Finally, an investigation into the non-uniform variation of the scatterer's material properties should be performed. This would determine their affect on the structure of the beam pattern from the sphere which may explain the poor results obtained with the 500 μm sphere.

APPENDIX A. MONOSTATIC DATA RESULTS

Frequency (kHz)	Aluminum Scattered Amplitude (mV)	Aluminum Corrected Incident Amplitude (mV)	Aluminum Normalized Amplitude	100 μm Scattered Amplitude (mV)	100 μm Corrected Incident Amplitude (mV)	100 μm Normalized Amplitude	500 μm Scattered Amplitude (mV)	500 μm Corrected Incident Amplitude (mV)	500 μm Normalized Amplitude
30	1.98	72.2	0.0197	1.41	76.4	0.0132	3.96	146.6	0.0193
32	2.37	89.1	0.0192	2.09	92.4	0.0162	2.13	184.2	0.0083
34	2.17	95.8	0.0163	1.08	95.3	0.0081	3.89	182.6	0.0152
36	2.18	109.8	0.0143	2.54	109.4	0.0166	5.49	212.2	0.0185
38	2.97	118.9	0.0180	4.12	116.7	0.0253	5.09	224.8	0.0162
40	2.69	135.4	0.0143	1.82	135.3	0.0096	6.10	255.0	0.0171
42	2.75	150.4	0.0132	5.71	151.9	0.0269	6.97	272.7	0.0183
44	1.98	174.8	0.0082	6.43	175.6	0.0262	7.31	302.2	0.0173
46	1.86	196.2	0.0068	4.68	198.5	0.0169	8.48	331.0	0.0183
48	5.60	225.4	0.0179	2.35	232.5	0.0072	10.16	381.1	0.0191
50	7.34	250.9	0.0211	4.24	258.9	0.0117	6.42	420.2	0.0109
52	9.17	283.0	0.0234	2.34	284.8	0.0059	5.20	462.7	0.0080
54	10.02	311.2	0.0232	6.80	303.3	0.0160	10.17	494.2	0.0147
56	10.78	344.9	0.0225	1.23	329.4	0.0027	12.92	542.6	0.0170
58	11.00	372.6	0.0213	5.92	361.3	0.0117	11.84	602.3	0.0141
60	11.65	407.1	0.0206	9.56	396.3	0.0173	11.19	676.4	0.0118
62	6.10	437.6	0.0100	10.40	433.1	0.0172	17.39	761.8	0.0163
64	4.61	467.4	0.0071	4.70	477.4	0.0070	24.20	864.8	0.0200
66	13.83	510.1	0.0195	8.15	530.7	0.0110	27.93	969.7	0.0206
68	17.41	565.3	0.0222	10.99	595.9	0.0132	30.08	1,080.5	0.0199
70	17.87	632.3	0.0204	7.31	669.3	0.0078	19.72	1,184.7	0.0119
72	23.18	710.7	0.0235	11.60	738.0	0.0112	24.06	1,312.3	0.0131
74	19.27	789.8	0.0176	17.87	798.0	0.0160	29.38	1,400.9	0.0150
76	20.32	847.8	0.0173	10.92	827.1	0.0094	32.12	1,471.0	0.0156
78	9.89	920.7	0.0077	4.36	869.6	0.0036	38.38	1,578.6	0.0174
80	13.52	1040.6	0.0094	11.56	984.2	0.0084	49.24	1,799.6	0.0196
82	26.46	1212.4	0.0157	2.86	1,181.4	0.0017	48.16	2,131.2	0.0162
84	35.31	1458.3	0.0174	16.26	1,425.2	0.0082	44.36	2,601.0	0.0122
86	46.48	1779.6	0.0188	25.23	1,740.3	0.0104	64.77	3,195.8	0.0145
88	63.57	2171.6	0.0211	14.13	2,137.7	0.0047	79.66	3,976.2	0.0143
90	69.29	2616.1	0.0191	43.72	2,604.8	0.0120	97.28	4,872.4	0.0143
92	61.70	3146.0	0.0141	74.19	3,164.8	0.0168	128.67	5,870.8	0.0157
94	54.42	3634.0	0.0108	58.89	3,718.8	0.0113	151.14	6,837.5	0.0158
96	68.43	3834.4	0.0129	37.77	3,992.6	0.0068	151.81	7,354.5	0.0148
98	53.58	3607.6	0.0107	48.47	3,835.2	0.0090	126.53	7,210.0	0.0126
100	56.15	3316.4	0.0122	35.40	3,558.4	0.0071	106.26	6,867.5	0.0111
102	72.82	3633.8	0.0144	11.87	3,808.8	0.0022	73.77	7,307.0	0.0072
104	93.49	4565.2	0.0148	6.04	4,605.6	0.0009	109.73	8,625.5	0.0091
106	92.14	5410.8	0.0123	24.91	5,364.4	0.0033	89.51	9,975.0	0.0064
108	80.72	5755.6	0.0101	57.30	5,629.6	0.0073	130.24	10,683.0	0.0087
110	92.62	5604.8	0.0119	65.85	5,534.8	0.0085	139.97	10,628.0	0.0094
112	97.44	5182.0	0.0135	28.33	5,151.6	0.0039	119.58	10,073.5	0.0085

Frequency (kHz)	Aluminum Scattered Amplitude (mV)	Aluminum Corrected Incident Amplitude (mV)	Aluminum Normalized Amplitude	100 μm Scattered Amplitude (mV)	100 μm Corrected Incident Amplitude (mV)	100 μm Normalized Amplitude	500 μm Scattered Amplitude (mV)	500 μm Corrected Incident Amplitude (mV)	500 μm Normalized Amplitude
114	96.93	4581.2	0.0152	38.35	4,595.6	0.0060	118.05	9,125.0	0.0093
116	79.54	3878.4	0.0148	48.85	3,927.0	0.0089	112.10	8,013.0	0.0100
118	71.32	3260.0	0.0158	24.81	3,269.8	0.0054	123.88	6,920.8	0.0128
120	50.71	2898.4	0.0126	10.50	3,008.6	0.0025	108.15	6,245.3	0.0124
122	36.51	2924.6	0.0090	28.56	2,930.4	0.0070	101.39	6,005.0	0.0121
124	44.15	3042.4	0.0105	22.79	3,030.4	0.0054	119.62	6,078.0	0.0141
126	61.34	3217.6	0.0137	18.33	3,179.8	0.0041	142.32	6,240.0	0.0163
128	74.04	3310.4	0.0161	32.47	3,251.4	0.0071	141.69	6,258.3	0.0162
130	78.00	3215.0	0.0175	28.93	3,144.4	0.0066	122.84	6,090.8	0.0144
132	70.86	3032.4	0.0168	—	2,935.0	—	119.41	5,806.3	0.0147
134	58.31	2902.6	0.0145	16.47	2,787.2	0.0042	126.25	5,488.0	0.0165
136	44.83	2781.8	0.0116	20.30	2,653.4	0.0055	120.71	5,142.0	0.0168
138	38.13	2616.4	0.0105	15.85	2,451.0	0.0046	102.76	4,747.1	0.0155
140	40.16	2361.8	0.0122	13.96	2,202.8	0.0045	81.74	4,352.2	0.0134
142	39.78	2127.1	0.0135	18.04	1,973.4	0.0065	66.25	3,965.6	0.0120
144	33.93	1943.0	0.0126	18.07	1,804.8	0.0072	55.41	3,611.2	0.0110
146	26.93	1796.5	0.0108	17.97	1,682.2	0.0076	49.04	3,344.4	0.0105
148	19.95	1655.3	0.0087	10.44	1,563.4	0.0048	44.13	3,063.8	0.0103
150	13.29	1481.7	0.0065	6.84	1,417.4	0.0035	41.93	2,757.6	0.0109

APPENDIX B. BISTATIC DATA RESULTS

30 kHz

Angle	Aluminum Scattered Amplitude (mV)	Aluminum Normalized Amplitude	100 μm Scattered Amplitude (mV)	100 μm Normalized Amplitude	500 μm Scattered Amplitude (mV)	500 μm Normalized Amplitude
90	2.33	0.0224	0.67	0.0066	1.50	0.0146
95	1.84	0.0177	0.69	0.0067	0.88	0.0086
100	2.76	0.0266	1.42	0.0138	0.34	0.0033
105	2.96	0.0286	2.18	0.0212	0.73	0.0071
110	2.99	0.0288	2.56	0.0250	1.07	0.0104
115	2.98	0.0288	1.89	0.0184	0.92	0.0090
120	2.90	0.0280	1.40	0.0137	1.13	0.0110
125	2.52	0.0243	1.11	0.0108	1.22	0.0119
130	2.23	0.0215	0.64	0.0062	0.34	0.0033
135	1.65	0.0159	0.86	0.0084	0.25	0.0024
140	1.72	0.0166	0.95	0.0092	1.41	0.0137
145	1.57	0.0152	1.55	0.0151	1.26	0.0123
150	1.79	0.0173	2.32	0.0226	0.67	0.0066
155	2.15	0.0208	1.65	0.0161	1.23	0.0120
160	1.91	0.0184	1.73	0.0168	1.33	0.0129
165	2.07	0.0199	2.38	0.0232	1.74	0.0169
170	2.24	0.0216	2.94	0.0287	1.41	0.0137
175	2.17	0.0209	4.01	0.0391	1.46	0.0142
180	2.24	0.0216	3.61	0.0351	1.43	0.0139
185	2.27	0.0219	3.64	0.0354	1.60	0.0156
190	2.05	0.0197	2.94	0.0286	1.31	0.0128
195	1.63	0.0157	2.10	0.0204	1.46	0.0142
200	1.47	0.0142	1.80	0.0175	1.21	0.0118
205	1.68	0.0162	1.56	0.0151	1.40	0.0137
210	1.51	0.0145	2.27	0.0221	1.26	0.0122
215	0.99	0.0095	2.08	0.0202	1.51	0.0147
220	1.76	0.0170	1.71	0.0167	1.08	0.0106
225	1.79	0.0173	1.39	0.0136	0.53	0.0052
230	1.92	0.0185	0.55	0.0053	0.17	0.0017
235	2.11	0.0204	0.15	0.0015	1.15	0.0112
240	2.88	0.0278	0.67	0.0066	1.18	0.0114
245	3.20	0.0309	1.45	0.0142	1.39	0.0136
250	3.36	0.0324	2.15	0.0209	1.35	0.0131
255	3.13	0.0302	2.34	0.0228	1.00	0.0098
260	3.42	0.0329	2.12	0.0207	0.78	0.0076
265	2.59	0.0249	1.46	0.0142	0.67	0.0065
270	1.33	0.0128	0.74	0.0072	0.91	0.0089
Incident	74.22		73.51		73.51	

60 kHz

Angle	100 µm		500 µm	
	Scattered Amplitude (mV)	Normalized Amplitude	Scattered Amplitude (mV)	Normalized Amplitude
90	10.95	0.0191	14.80	0.0136
95	8.57	0.0150	10.80	0.0099
100	6.40	0.0112	10.03	0.0092
105	4.35	0.0076	10.84	0.0099
110	10.31	0.0180	12.09	0.0111
115	12.06	0.0210	11.85	0.0109
120	11.01	0.0192	15.14	0.0139
125	3.13	0.0055	15.46	0.0142
130	3.32	0.0058	15.30	0.0140
135	6.61	0.0115	11.25	0.0103
140	5.59	0.0098	8.83	0.0081
145	6.14	0.0107	14.33	0.0131
150	4.15	0.0072	12.17	0.0112
155	3.65	0.0064	14.61	0.0134
160	4.58	0.0080	11.92	0.0109
165	2.66	0.0046	12.85	0.0118
170	4.46	0.0078	7.37	0.0068
175	9.05	0.0158	11.39	0.0104
180	11.72	0.0205	15.50	0.0142
185	10.90	0.0190	13.95	0.0128
190	8.91	0.0155	12.59	0.0115
195	5.23	0.0091	16.32	0.0150
200	2.63	0.0046	16.71	0.0153
205	4.25	0.0074	14.02	0.0129
210	6.15	0.0107	12.46	0.0114
215	8.00	0.0140	13.03	0.0119
220	6.37	0.0111	10.87	0.0100
225	5.42	0.0095	12.33	0.0113
230	5.62	0.0098	11.62	0.0106
235	4.04	0.0070	13.63	0.0125
240	5.60	0.0098	14.17	0.0130
245	8.64	0.0151	12.53	0.0115
250	9.14	0.0159	13.31	0.0122
255	5.98	0.0104	9.77	0.0090
260	0.81	0.0014	14.16	0.0130
265	6.66	0.0116	14.40	0.0132
270	9.14	0.0160	14.51	0.0133
Incident	410.05		780.75	

90 kHz

Angle	100 μm Scattered Amplitude (mV)	100 μm Normalized Amplitude	500 μm Scattered Amplitude (mV)	500 μm Normalized Amplitude
90	51.20	0.0127	42.37	0.0066
95	39.37	0.0098	77.50	0.0120
100	17.89	0.0044	225.41	0.0349
105	47.56	0.0118	65.48	0.0101
110	39.39	0.0098	82.71	0.0128
115	10.34	0.0026	136.89	0.0212
120	19.01	0.0047	112.68	0.0175
125	33.49	0.0083	53.00	0.0082
130	26.09	0.0065	35.81	0.0055
135	13.15	0.0033	55.51	0.0086
140	16.89	0.0042	36.87	0.0057
145	35.55	0.0088	41.07	0.0064
150	33.40	0.0083	37.97	0.0059
155	34.16	0.0085	44.34	0.0069
160	36.12	0.0090	66.64	0.0103
165	36.49	0.0090	58.09	0.0090
170	39.45	0.0098	40.60	0.0063
175	51.11	0.0127	61.83	0.0096
180	56.62	0.0140	67.19	0.0104
185	50.90	0.0126	76.02	0.0118
190	42.01	0.0104	22.14	0.0034
195	38.67	0.0096	66.06	0.0102
200	38.45	0.0095	53.77	0.0083
205	36.68	0.0091	59.32	0.0092
210	34.31	0.0085	36.41	0.0056
215	26.59	0.0066	32.11	0.0050
220	17.33	0.0043	47.76	0.0074
225	23.49	0.0058	37.85	0.0059
230	36.83	0.0091	59.20	0.0092
235	37.65	0.0093	49.09	0.0076
240	16.85	0.0042	51.08	0.0079
245	20.13	0.0050	47.70	0.0074
250	40.02	0.0099	45.56	0.0071
255	34.82	0.0086	49.62	0.0077
260	27.47	0.0068	56.56	0.0088
265	29.21	0.0072	73.82	0.0114
270	39.30	0.0097	69.75	0.0108
Incident	2886.0		4620.8	

120 kHz

Angle	100 μm		500 μm	
	Scattered Amplitude (mV)	Normalized Amplitude	Scattered Amplitude (mV)	Normalized Amplitude
90	51.31	0.0117	38.77	0.0106
95	43.76	0.0099	28.49	0.0078
100	22.59	0.0051	11.18	0.0031
105	42.98	0.0098	20.21	0.0055
110	27.04	0.0061	29.50	0.0081
115	34.00	0.0077	26.58	0.0073
120	35.89	0.0082	36.97	0.0101
125	48.33	0.0110	28.56	0.0078
130	43.22	0.0098	17.68	0.0048
135	33.03	0.0075	19.39	0.0053
140	24.26	0.0055	23.07	0.0063
145	33.20	0.0075	24.95	0.0068
150	39.00	0.0089	18.48	0.0051
155	29.31	0.0067	24.74	0.0068
160	18.77	0.0043	27.82	0.0076
165	17.43	0.0040	26.91	0.0074
170	26.23	0.0060	30.22	0.0083
175	43.54	0.0099	26.30	0.0072
180	54.23	0.0123	31.63	0.0087
185	53.13	0.0121	22.21	0.0061
190	44.05	0.0100	41.32	0.0113
195	29.80	0.0068	45.13	0.0124
200	17.51	0.0040	26.00	0.0071
205	41.77	0.0095	36.59	0.0100
210	44.56	0.0101	35.17	0.0096
215	31.83	0.0072	29.53	0.0081
220	32.51	0.0074	31.48	0.0086
225	40.28	0.0092	26.86	0.0074
230	36.76	0.0084	27.25	0.0075
235	18.17	0.0041	31.57	0.0086
240	33.11	0.0075	28.24	0.0077
245	23.39	0.0053	39.94	0.0109
250	21.27	0.0048	42.82	0.0117
255	30.41	0.0069	15.78	0.0043
260	17.81	0.0040	16.91	0.0046
265	46.02	0.0105	28.25	0.0077
270	27.73	0.0063	42.53	0.0117
Incident	3148.6		2612.0	

150 kHz

Angle	Aluminum		100 μm		500 μm	
	Scattered Amplitude (mV)	Normalized Amplitude	Scattered Amplitude (mV)	Normalized Amplitude	Scattered Amplitude (mV)	Normalized Amplitude
90	31.80	0.0390	14.22	0.0069	3.16	0.0017
95	28.28	0.0346	23.70	0.0115	10.45	0.0056
100	3.84	0.0047	3.94	0.0019	4.70	0.0025
105	11.00	0.0135	5.43	0.0026	10.12	0.0054
110	15.08	0.0185	9.29	0.0045	7.91	0.0042
115	13.85	0.0170	7.66	0.0037	9.73	0.0052
120	12.54	0.0154	9.19	0.0044	12.08	0.0065
125	27.40	0.0336	9.34	0.0045	8.54	0.0046
130	15.04	0.0184	7.74	0.0037	9.24	0.0049
135	30.90	0.0378	13.59	0.0066	7.67	0.0041
140	4.89	0.0060	15.24	0.0074	7.73	0.0041
145	23.90	0.0293	0.23	0.0001	9.86	0.0053
150	23.41	0.0287	4.73	0.0023	9.71	0.0052
155	26.68	0.0327	11.87	0.0057	3.33	0.0018
160	33.31	0.0408	8.62	0.0042	11.70	0.0063
165	23.45	0.0287	15.26	0.0074	3.70	0.0020
170	15.03	0.0184	18.64	0.0090	5.96	0.0032
175	29.77	0.0365	15.42	0.0075	4.63	0.0025
180	38.15	0.0467	18.68	0.0090	6.58	0.0035
185	17.47	0.0214	8.66	0.0042	13.05	0.0070
190	33.76	0.0413	16.71	0.0081	6.60	0.0035
195	18.08	0.0221	19.46	0.0094	15.67	0.0084
200	19.80	0.0242	20.20	0.0098	8.85	0.0047
205	12.46	0.0153	17.20	0.0083	6.76	0.0036
210	32.76	0.0401	13.13	0.0064	5.49	0.0029
215	8.70	0.0107	13.45	0.0065	4.83	0.0026
220	16.79	0.0206	11.81	0.0057	9.90	0.0053
225	8.93	0.0109	6.94	0.0034	9.17	0.0049
230	33.38	0.0409	9.36	0.0045	12.60	0.0067
235	1.36	0.0017	11.79	0.0057	10.98	0.0059
240	18.24	0.0223	10.84	0.0052	11.07	0.0059
245	9.89	0.0121	8.44	0.0041	14.90	0.0080
250	8.46	0.0104	6.36	0.0031	9.24	0.0049
255	6.12	0.0075	15.67	0.0076	13.97	0.0075
260	21.72	0.0266	21.24	0.0103	13.83	0.0074
265	25.74	0.0315	16.22	0.0078	6.39	0.0034
270	15.17	0.0186	1.75	0.0008	15.89	0.0085
Incident	545.35	571.48	1479.9		1337.5	

APPENDIX C. INPUTS TO KARGL'S PROGRAM

Monostatic Inputs			
	Aluminum	**100 μm**	**500 μm**
External Fluid (Water)			
Density, ρ_f	998.665	998.665	998.665
Bulk Modulus, K_f	2.17293×10^9	2.17293×10^9	2.17293×10^9
Viscosity, η	0.0	0.0	0.0
Internal Fluid			
Density, ρ_{f0}	2700	998.665	998.665
Bulk Modulus, K_{f0}	8.078×10^{10}	2.17293×10^9	2.17293×10^9
Viscosity, η_0	0.001	0.001	0.001
External Medium (Water)			
Density, ρ_f	998.665	998.665	998.665
Solid Bulk Modulus, K_s	$(2.17293\times10^9, 0.0)$	$(2.17293\times10^9, 0.0)$	$(2.17293\times10^9, 0.0)$
Lattice Bulk Modulus, K_B	$(2.25\times10^5, 0.0)$	$(2.17293\times10^5, 0.0)$	$(2.17293\times10^5, 0.0)$
Shear Modulus, μ	(1.0, 0.0)	(1.0, 0.0)	(1.0, 0.0)
Tortuosity, α	1.65	1.65	1.65
Porosity, β	0.999999	0.999999	0.999999
Permeability, k_d	1.0	1.0	1.0
Internal Medium (Sphere)			
Density, ρ_0	2700	2231	2231
Solid Bulk Modulus, K_{s0}	$(8.078\times10^{10}, 0.0)$	$(3.5\times10^{10}, 0.0)$	$(3.5\times10^{10}, 0.0)$
Lattice Bulk Modulus, K_{B0}	$(8.078\times10^{10}, 0.0)$	$(2.96\times10^9, 0.0)$	$(2.87\times10^9, 0.0)$
Shear Modulus, μ_0	$(2.677\times10^{10}, 0.0)$	$(2.81\times10^9, 0.0)$	$(2.72\times10^9, 0.0)$
Tortuosity, α_0	1.65	1.65	1.65
Porosity, β_0	0.321	0.306	0.305
Permeability, k_{d0}	1.0×10^{-16}	6.53×10^{-12}	5.74×10^{-11}
Miscellaneous			
a_p	1.0×10^{-5}	1.0×10^{-5}	1.0×10^{-5}
a_{p0}	1.0×10^{-5}	1.0×10^{-5}	1.0×10^{-5}
dfreq	100	100	100
max. freq.	150000	150000	150000
radius	0.0382	0.0344	0.0346
distance	0.75	0.75	0.75
hash	0	0	0
nstart	0	0	0
nend	75	75	75

Bistatic Inputs			
	Aluminum	**100 μm**	**500 μm**
External Fluid (Water)			
Density, ρ_f	998.665	998.665	998.665
Bulk Modulus, K_f	2.17293×10^9	2.17293×10^9	2.17293×10^9
Viscosity, η	0.0	0.0	0.0
Internal Fluid			
Density, ρ_{f0}	2700	998.665	998.665
Bulk Modulus, K_{f0}	8.078×10^{10}	2.17293×10^9	2.17293×10^9
Viscosity, η_0	1.0	0.001	0.001
External Medium (Water)			
Density, ρ_f	998.665	998.665	998.665
Solid Bulk Modulus, K_s	$(2.17293\times10^9, 0.0)$	$(2.17293\times10^9, 0.0)$	$(2.17293\times10^9, 0.0)$
Shear Modulus, μ	(1.0, 0.0)	(1.0, 0.0)	(1.0, 0.0)
Porosity, β	0.999999	0.999999	0.999999
Permeability, k_d	1.0	1.0	1.0
Internal Medium (Sphere)			
Density, ρ_0	2700	2231	2231
Solid Bulk Modulus, K_{s0}	$(8.078\times10^{10}, 0.0)$	$(3.5\times10^{10}, 0.0)$	$(3.5\times10^{10}, 0.0)$
Shear Modulus, μ_0	$(2.677\times10^{10}, 0.0)$	$(2.6\times10^{10}, 0.0)$	$(2.6\times10^{10}, 0.0)$
Porosity, β_0	1.0×10^{-6}	0.306	0.305
Permeability, k_{d0}	1.0×10^{-16}	6.53×10^{-12}	5.74×10^{-11}
Miscellaneous			
nfreq	2	5	5
freqmin	30000	30000	30000
dfreq	120000	30000	30000
x1min	0	0	0
x1max	50	50	50
radius	0.382	0.0344	0.0346
distance	1.0	0.75	0.75
hash	1	1	1
nstart	0	0	0
nend	75	75	75
exp	1	1	1
exp0	1	0	0
# of angles	361	361	361
Experimental K_{b0}	—	$(2.96\times10^9, 0.0)$	$(2.87\times10^9, 0.0)$
Experimental μ_0	—	$(2.81\times10^9, 0.0)$	$(2.72\times10^9, 0.0)$

LIST OF REFERENCES

(Biot, 1956a): M. A. Biot, "Theory of propagation of elastic waves in a fluid-saturated porous solid. I. Low-frequency range," *J. Acoust. Soc. Am.* **28**, pp. 168-178, 1956.

(Biot, 1956b): M. A. Biot, "Theory of propagation of elastic waves in a fluid-saturated porous solid. II. Higher frequency range," *J. Acoust. Soc. Am.* **28**, pp. 179-191, 1956.

(Garrett, 1990): S. L. Garrett, "Resonant acoustic determination of elastic moduli, " *J. Acoust. Soc. Am.* **88**, pp. 210-221, 1990.

(Hewlett-Packard): "The Fundamentals of Signal Analysis", Application Note 243, Hewlett-Packard Company, 1989.

(Huskey, 1993): T. W. L. Huskey, "Scattering of Underwater Sound from a Porous Solid Sphere," Thesis, Naval Postgraduate School, Monterey, CA, 1993.

(Kargl and Lim): S. G. Kargl and R. Lim, "A transition-matrix formulation of scattering in homogeneous, saturated, porous media," *J. Acoust. Soc. Am.* **94**, pp. 1527-1550, 1993.

(Kinsler et al.): L. E. Kinsler, A. R. Frey, A. B. Coppens, J. V. Sanders, *Fundamentals of Acoustics, Third Edition*, Wiley, New York, 1982.

(Sears, Salinger): F. W. Sears, G. L. Salinger, *Thermodynamics, Kinetic Theory, and Statistical Thermodynamics, Third Edition,* Addison-Wesley, Reading, MA, 1975.

INITIAL DISTRIBUTION LIST

1. Defense Technical Information Center 2
   Cameron Station
   Alexandria, Virginia 22304-6145

2. Library, Code 52.. 2
   Naval Postgraduate School
   Monterey, California 93943-5002

3. Commander 3
   Attn.: Doug Todoroff
   Naval Coastal Systems Station
   Panama City, Florida 32407-7001

4. Steven R. Baker, Code PH/BA.. 2
   Naval Postgraduate School
   Monterey, California 93943-5002

5. Steven G. Kargl 1
   University of Washington, Applied Physics Laboratory
   Seattle, Washington 98105

6. Clyde Scandrett, Code MA/SD 1
   Naval Postgraduate School
   Monterey, California 93943-5002

7. Dr. David L. Johnson 1
   Schlumberger-Doll Research
   Old Quarry Road
   Ridgefield, Connecticut 06877-4108

8. Dr. Nicholas Chotiros.. 1
   University of Texas, Applied Physics Laboratory
   Austin, Texas 78712

9. Dr. Robert D. Stoll 1
   Columbia University, Lamont-Doherty Earth Obs.
   Palisades, New York 10964

10. Dr. Tokuo Yamamoto.. 1
    University of Miami, Rosensteil School of Marine/Atmos. Science
    Miami, Florida 33149

11. Jim Eagle, Code 37 1
Naval Postgraduate School
Monterey, California 93943-5002

12. Lieutenant Martin E. Pace 1
5175 Nordic Court N.
Keizer, Oregon 97303-7510